Photoabsorption of potassium clusters isolated in helium droplets: From discrete electronic transitions to collective resonances

Roman Messner, Robert di Vora, Wolfgang E. Ernst, and Florian Lackner*
Institute of Experimental Physics, Graz University of Technology, Petersgasse 16, 8010 Graz, Austria

(Received 24 September 2021; revised 14 March 2022; accepted 15 April 2022; published 24 May 2022)

Photoabsorption spectra of neutral potassium clusters in helium nanodroplets are recorded by depletion spectroscopy using a supercontinuum laser source equipped with a variable bandpass filter. The results provide insight into the evolution of electronic spectra from molecular transitions to localized surface plasmon resonances in nanometer-sized clusters. Size selected spectra for potassium clusters K_n are acquired from $n = 2$–110. Indications for the transition from molecularlike absorption to a collective resonance are already observed below $n = 20$. For larger clusters, a splitting of the plasmon mode into two components is observed at around $n = 600$. Supported by simulations, this is explained by the presence of nonspherical potassium nanoparticles grown via multicenter aggregation inside the helium droplets. The presented supercontinuum laser-based experimental approach provides a new route for the mass-selective spectroscopic characterization of different materials and material combinations isolated in helium nanodroplets in a size regime ranging from single atoms and molecules to small sub-10-nm particles.

DOI: 10.1103/PhysRevResearch.4.023148

I. INTRODUCTION

Metal clusters have attracted strong interest for several decades. Early measurements of the geometric and electronic structure of metal clusters aimed at the exploration of an intermediate state of matter between free molecules and solid state. Questions, such as the transition from a molecular structure to the formation of a crystal lattice or the convergence of the cluster size-dependent ionization energy to the work function of the corresponding solid were addressed, see, for example, the book on *Clusters of Atoms and Molecules* edited by Haberland [1]. In the past two decades the optical properties of metallic nanoparticles gained particular interest because of the size-dependent shift of plasmonic resonances [2] due to quantum confinement, which becomes particularly important in the sub-10-nm size regime. Tunability of the optical absorption may allow for many applications from surface enhanced Raman spectroscopy [3,4] to plasmon enhanced sensing and solar energy conversion [5–8]. Localized surface plasmon resonances (LSPR), the key feature of plasmonic nanoparticles [9], originate from collective oscillations of conduction-band electrons. In this regard, it is important to determine the particle size from which onward, the optical absorption is no longer governed by transitions between molecular electronic states but can be described as LSPR.

Alkali clusters have been an important model system for first studies of the optical absorption of metal clusters. Photodepletion spectroscopy emerged as the prime method for their investigation in the late 1980s [10,11]. Among the investigations of potassium clusters, the focus was on charged species K_n^+. Spectra for selected sizes of $n = 9$, 11, 14–21, 500, and 900 [12–14] have been reported. The corresponding spectra are dominated by a broad feature that peaks at about 642 nm for K_9^+ and that shifts toward the blue with increasing cluster size where 605 nm is reported for K_{900}^+. The stability of both neutral and charged K_n^+ clusters has been investigated [15–18], and magic numbers were found for the 8, 20, and 40 electron systems [17]. Experiments on potassium clusters comprising more than 900 atoms are scarce. Results for nanometer-sized particles have been obtained by matrix isolation spectroscopy [19,20] and photoelectron spectroscopy [21,22].

Alkali clusters already as small as trimers exhibit signs of the delocalization of valence electrons. For example, the hyperfine structure and electric dipole moment in the electronic ground state of the sodium trimer [23] showed a strong agreement with the electronic shell model for alkali clusters [11,24]. For tetramers features associated with a collective resonance were observed [10,11].

Alkali atoms, dimers, and trimers, are among the best-studied complexes isolated in helium nanodroplets [25–30]. Time-of-flight mass spectra of potassium clusters in helium nanodroplets were published in Refs. [31–33]. A peculiarity of alkali clusters is their location: Whereas molecules and small clusters reside at the surface, beyond a certain size the clusters fully submerge into the droplet [34]. For K_n, this transition occurs at about $n = 80$ [32]. Whereas the electronic spectra for alkali complexes in helium nanodroplets beyond the trimer are hitherto unknown, the plasmon resonance of small Ag_8 clusters in helium nanodroplets has been investigated previously [35,36]. Studies of the plasmon resonance for broader size distributions have been reported for Ag and Cu clusters [37,38].

*florian.lackner@tugraz.at

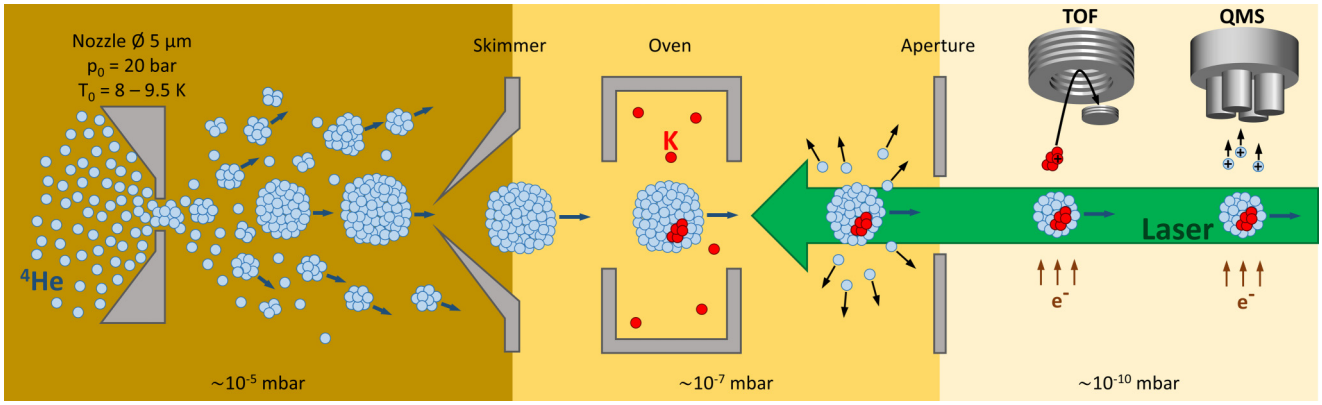

FIG. 1. Sketch of the experiment: Helium droplets are formed by expanding cold pressurized helium gas through a small orifice. Subsequently, potassium atoms are added to the droplets where they coagulate and form clusters. The supercontinuum laser (green) is oriented antiparallel to the droplet beam and scanned from 500 to 840 nm. If the laser frequency is resonant with a transition of the accommodated complex, the deposited excitation energy is dissipated by the evaporation of helium atoms, which translates into a reduced cross section for electron impact ionization. This results in a depletion signal, which is either probed directly at the corresponding potassium cluster mass for K_n with n up to 110 using a TOF mass spectrometer or at the He ($m = 4$) mass window using a QMS detector.

In this paper, we report absorption spectra for neutral potassium clusters K_n that provide insight into the size regime where molecular absorption bands evolve into plasmon resonances. Indications for the transition between these two regimes are identified already below $n = 20$. Two types of experiments are presented both based on laser spectroscopy with a supercontinuum source that can be scanned from 500 to 840 nm: The first part of this paper reports on results obtained with a time-of-flight mass spectrometer (TOF MS), which enables the acquisition of beam depletion spectra for individual mass channels for K_n up to $n = 110$. The size range from single atoms up to clusters comprising several thousands of atoms is the subject of the second part of this paper. In this case, a quadrupole mass spectrometer (QMS) is used to record beam depletion spectra for potassium clusters, averaging over the adjusted size distribution. This approach reveals insight into the structure of complexes isolated in helium droplets: At about K_{600} a bifurcation of the plasmon mode is observed, owed to the peculiar synthesis environment that favors the formation of elongated nanoparticles under certain conditions.

II. EXPERIMENTAL DETAILS

A sketch of the experiment is shown in Fig. 1 with the employed helium droplet apparatus described in detail elsewhere [39]. Cold helium gas at a pressure of 20 bars is expanded through a 5 μm nozzle into high vacuum, which results in the condensation of helium nanodroplets that provide a cold, inert, and superfluid matrix (0.4 K) [40,41]. In the pickup region, potassium is evaporated using a resistively heated fused-silica crucible. Dopant atoms are collected by the droplets and agglomerate to clusters [42,43]. The resulting cluster size distribution is controlled by adjusting the potassium crucible temperature between about 370 and 470 K as well as the helium pressure and temperature, i.e., the size of the helium droplets [40,41].

Potassium clusters are probed *in situ* by beam depletion spectroscopy with the laser aligned antiparallel to the droplet beam. A novel aspect of the experimental setup is the employed high power supercontinuum laser (NKT SuperK Extreme). The laser is equipped with a variable bandpass filter (NKT SuperK Varia) and can be tuned from 500 to 840 nm with a minimum bandwidth of 6 nm. With an 80-Mhz repetition rate, the laser represents a quasi-cw source. In contrast to a pulsed optical parametric oscillator or dye laser system, this enables a straightforward combination with a TOF MS operated in the electron impact ionization mode and the implementation of lock-in technology (@62 Hz) for an improved signal-to-noise ratio in combination with a QMS. The laser power is stabilized and kept constant over the entire spectral range up to 30 mW have been employed with a beam diameter of about 2 mm.

The excitation of potassium clusters results in a depletion of the respective mass channel, which allows for the recording of mass resolved depletion spectra for K_n clusters up to $n = 110$ using the TOF MS. Furthermore, the energy absorbed by the excited potassium clusters is rapidly dissipated by the evaporation of helium atoms [44]. This process translates into a decrease in helium flux, which is detected by the QMS detector set to the He mass (4 u). The helium matrix is transparent for the laser [40], thus, the depletion signal is proportional to the photoabsorption of the isolated species.

III. RESULTS AND DISCUSSION

Figure 2 presents absorption spectra obtained for small potassium clusters K_n up to $n = 110$, recorded with the TOF MS. The bottom panel shows a two-dimensional (2D) representation of individual spectra, providing an overview of the data set, whereas selected spectra between $n = 2$ and 20 are shown in the top panel. For each spectrum, a TOF mass window corresponding to a single cluster size has been selected, i.e., the windows are separated by $\Delta m = 39$ (see Appendix A). The recorded ion yield as a function of the wavelength is plotted, divided by the ion yield obtained for each mass window in the absence of the depletion laser. The mean diameter of the employed helium nanodroplets He_N corresponds to about 20 nm (source conditions: 9.5 K

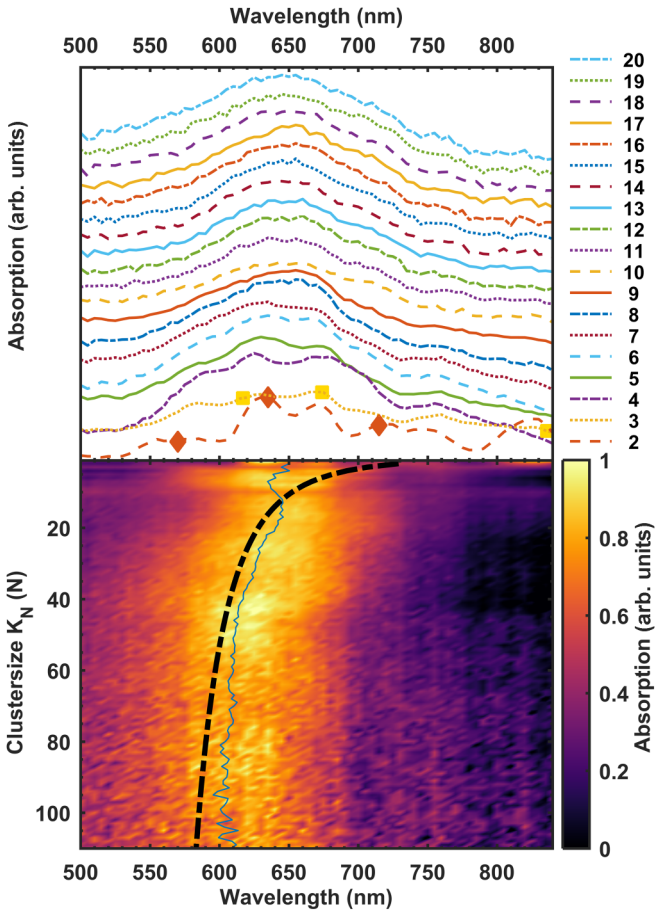

FIG. 2. Compilation of absorption spectra recorded for potassium clusters isolated in helium nanodroplets with 20 nm mean diameter, obtained by beam depletion spectroscopy using the TOF mass spectrometer. The laser is power-stabilized (30 mW) over the shown wavelength range with a bandwidth of 20 nm. Bottom panel: 2D representation of the recorded spectra for K_n clusters with sizes up to $n = 110$, yellow regions correspond to maximum absorption (i.e., depletion). The black dashed line represents the calculated plasmon peak position using the Kresin model described in Ref. [10]. The solid blue line marks the position of the peak maximum for each cluster size, obtained from a Gaussian fit. Top panel: Individual spectra of the recorded data set are shown for K_n from $n = 2$ up to $n = 20$, each line style and color combination corresponds to a certain cluster size (see the legend). The positions of known K_2 and K_3 transitions are marked by diamonds and squares, respectively [26,27,29,30,45,46].

and 20 bars). Features in the dimer and trimer spectra can be readily assigned based on comparison to literature, the corresponding band positions are marked in the figure (top panel) and listed in Table I in Appendix B [26,27,29,30,45,46]. At the chosen doping conditions only very few singly doped He_N are present and the potassium D lines ($4\,^2P \leftarrow 4\,^2S$) at around 765 nm were not observed unless low doping was intentionally chosen (see below Fig. 3). The strongest observed peak corresponds to the singlet K_2 $1\,^1\Pi_u \leftarrow 1\,^1\Sigma_g^+$ transition at about 635 nm. Note that trimer transitions can also be observed in the dimer spectrum, as best seen for the K_3 $1\,^4A_1'' \leftarrow 1\,^4A_2'$ transition. This suggests that fragmentation of clusters can affect the recorded spectra as discussed in more detail below. Furthermore, it is known that alkali dimers and trimers can dissociate and desorb from the droplet surface upon photoexcitation [27]. With increasing cluster size, a broad structure that spans from 550 to 750 nm becomes dominant, attributed to the emerging collective resonance. However, structured moleculelike features on top can be identified up to around $n = 9$.

The main depletion feature visible in Fig. 2 (yellow—maximum absorption), bottom panel, corresponds to a broad structure that peaks at 650 nm for small clusters and which shifts toward shorter wavelength with increasing cluster size. The position of the peak maximum as a function of cluster size, obtained from a Gaussian fit, is represented by the blue line (see also Fig. 6 in Appendix C). The same feature is observed over an even larger size range shown in Fig. 3, *vide infra*, in the data set recorded with the QMS detector. In Fig. 2, which shows the mass selected TOF MS spectra, the position of this feature remains fairly constant beyond K_{50}, in particular, no anomaly is observed around K_{80} where the transition between surface and bulk location of the clusters occurs.

In Ref. [32], the location of potassium clusters was inferred based on the prevailing ionization mechanism: Whereas Penning ionization is important for species close to the surface, ionization of species inside the droplet is governed by a charge hopping mechanism. The latter requires the presence of He ions in the droplet, which can only be created if the kinetic energy of the ionizing electrons is beyond 24 eV. In contrast, Penning ionization is mediated by metastable He atoms, which are already formed below 24 eV. However, in our setup 89 eV are used as ionization energy and, consequently, the electron impact ionization scheme is insensitive to the cluster location. We note that, *a priori*, it is not clear if a surface location would give rise to a significantly different absorption spectrum: Clusters are considered to reside in a dimple structure at the surface [47], i.e., also at the surface they are surrounded by the liquid helium, and a matrix shift applies. Thus, differences in the absorption spectra between both cases may be not as dramatic as expected from ion impact ionization experiments. Here, density functional theory calculations could provide insight into the structure of a potassium cluster and the surrounding helium at the droplet surface and the expected absorption spectrum [48].

The black dashed line in the bottom panel of Fig. 2 represents the predicted position of the collective resonance for neutral potassium clusters as a function of their size based on the theoretical model presented by Kresin in Ref. [10]. Here, the bulk parameters listed in Ref. [10] are used, which dictate the value of the plasmon peak position towards which large clusters converge. The redshift with decreasing cluster size is explained by the spill out of electrons. The measurements confirm the peak shift qualitatively, which can be seen by comparing the Kresin model result (dashed black line) with the peak maximum as a function of cluster size (solid blue line) in the bottom panel of Fig. 2 (see also Appendix C, Fig. 6).

It is important to emphasize that although the TOF MS detects charged clusters, it is the neutral clusters that are excited and depleted prior to ionization. This plays a role

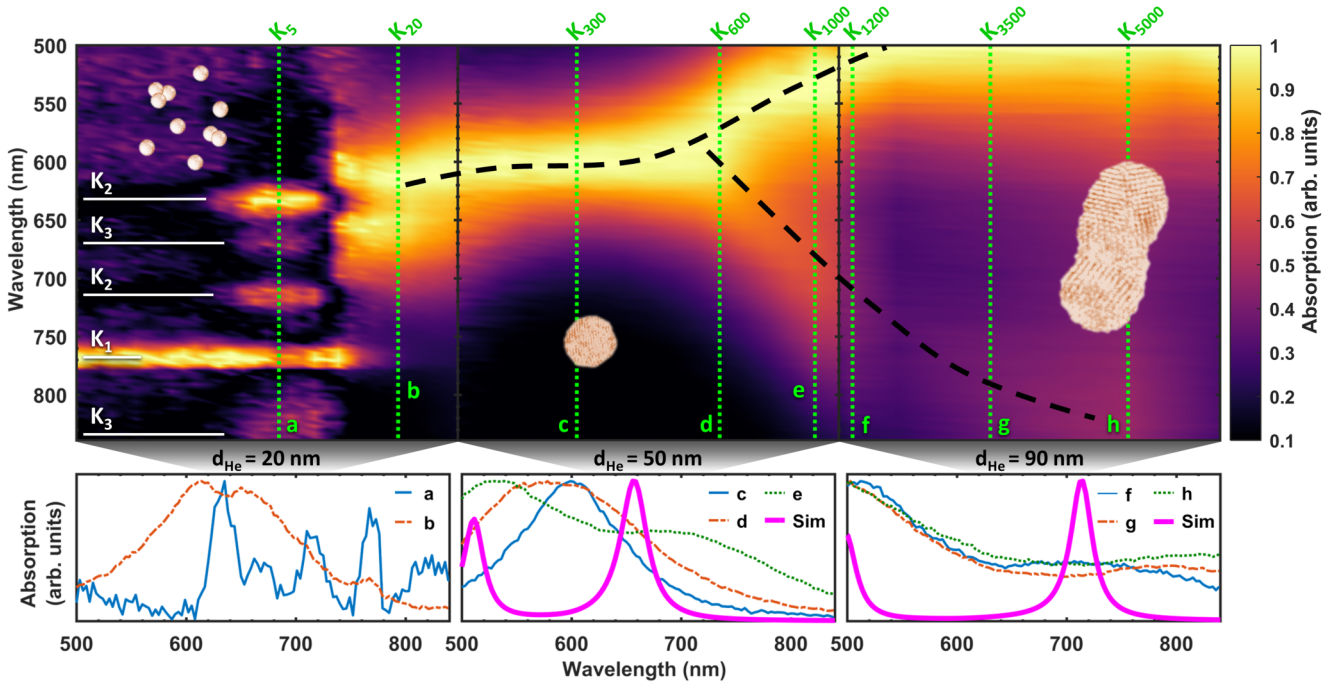

FIG. 3. Compilation of normalized absorption spectra recorded with the QMS detector for K_n cluster sizes ranging from single atoms to elongated nanostructures. Helium nanodroplets with diameters d_{He} of 20, 50, and 90 nm have been employed, which provide access to different K_n size regimes. The black dashed line marks the position of the absorption maximum. Artistic impressions of possible particle forms in different size regimes are indicated in the figure. Vertical dashed green lines mark the position of selected spectra shown in the three panels at the bottom, and white horizontal lines mark the identified atomic and molecular absorption bands. Simulated absorption spectra for $\sim K_{1000}$ and $\sim K_{3500}$ are labeled as "sim."

for small clusters and can be estimated by the model in Ref. [10]: For example, the peak positions for the 20 electron systems, K_{20} and K_{21}^+ correspond to 1.96 eV (633 nm) and 2.00 eV (620 nm), respectively, i.e., a difference of 13 nm. The maximum for K_{20} in the spectrum in Fig. 2 is at 645 nm, redshifted by 19 nm with respect to the charged cluster, in reasonable agreement with the value expected from the calculation.

In mass spectroscopic detection of clusters, fragmentation of the original clusters may distort the measured size distribution due to excess energy provided by the ionization source. For molecules and clusters inside helium droplets, ionization has been shown to occur via both a charge hopping process or Penning ionization with helium as intermediate rather than direct electron impact [49]. Helium droplets are known to alter fragmentation patterns observed for isolated molecules [50]. For some species, it has been shown that the low-temperature environment can suppress certain fragmentation channels [51]. However, typically, in the case of electron impact ionization fragmentation cannot be neglected, even for fully submerged clusters as the example of Ag_8 shows [36]. Thus, also for potassium it can be expected that fragmentation affects the recorded absorption spectra obtained with the TOF MS [32]. This could explain the absence of additional structures for K_n between $n = 8$ and 20, which may be expected from geometry and symmetry considerations in the cold helium droplet environment [11]. Furthermore, it cannot be excluded that fragmentation contributes to a broadening of the observed absorption peak features. However, effects, such as the redshift with decreasing cluster size, are not obscured by fragmentation and are still well captured.

Absorption spectra of potassium clusters starting from single atoms up to clusters K_n comprising several thousands of atoms, i.e., far beyond $n = 110$, are recorded using the QMS. As the detector is set to the ^{4}He mass window, information about individual mass channels is lost and the spectra are composed of the accumulated absorption of all clusters within the adjusted size distribution [37]. Note that in this case fragmentation processes that occur during electron impact ionization do not affect the measurements.

The corresponding absorption spectra are presented in Fig. 3, recorded for three different droplet sizes with a mean diameters of about 20, 50, and 90 nm, created at source conditions of 20 bars and 9.5, 9, and 8 K, respectively [52]. The shown 2D plots are composed of individual spectra recorded for different potassium pickup temperatures, the cluster size increases from left to right. Each spectrum has been normalized to the peak maximum. By arranging the panels for each droplet size next to each other, the evolution from molecular transitions to collective plasmon modes can be followed over a wide range of cluster sizes. Selected slices of the 2D plot are shown below with the mean estimated cluster sizes annotated in green on top. As described in Appendix D, the cluster size estimation is based on the decrease in the He signal caused by the release of binding energy during cluster formation.

For small helium nanodroplets and low potassium pickup temperatures, the spectrum (a) is dominated by molecular absorption features with the D lines of potassium atoms (760 nm) as the most prominent structure. With increasing

potassium doping level (b), a broad structured band emerges, which is attributed to the LSPR. The dashed black line marks the position of the peak maximum of this feature. The transition from the molecular to the plasmon regime proceeds abrupt with increasing pickup level and occurs already for small mean potassium cluster sizes K_n, below $n = 20$, in good agreement with the TOF MS measurements.

Another notable feature in the small cluster region, visible in spectrum (b), is the presence of dips in the broad absorption feature at the position of dimer and trimer transitions. Considering the geometry of the experiment (Fig. 1), this is tentatively attributed to molecules that desorb during the cluster formation process upon excitation. The additional feature at the monomer transition in this spectrum may be an indication for the presence of isolated atoms in addition to clusters, similar to observations reported in Refs. [27,53].

For larger helium nanodroplets the maximum size of the potassium clusters that can be accommodated is increased. At a droplet diameter of 50 nm a regime is reached where predominantly nanoparticles are formed and a single LSPR peak is prevailing. For potassium clusters K_n with a mean size of $n = 300$ (c) the peak maximum is located at 600 nm. This is in good agreement with previous results that report an absorption band maximum at 611 and 605 nm for K^+_{500} and K^+_{900} [14], respectively. Note that although the peak position remains fairly constant around K_{300} (c), with only a slight shift to the blue with increasing particle size, the absolute absorption increases considerably (not visible in the normalized spectra).

At highest doping levels a surprising behavior is observed: With increasing cluster size, a bifurcation occurs (e). The splitting of the plasmon band into two components, which sets in at around K_{600} (d), is interpreted as a transition from spherical to elongated potassium clusters. With increasing cluster size [(f) and (g)] the separation of the two peaks increases. Eventually, the low-energy band moves out of range for the employed laser, the high photon energy band settles slightly below 500 nm. Note that due to the normalization of the spectra to the maximum depletion value, i.e., to the wing of the plasmon peak in (g) and (h), the low-energy feature appears to increase with cluster size in the right panel.

The presence of multiple plasmon modes is typical for nonspherical elongated particles [54–58]. For nanorods, for example, a high-energy transversal mode and a longitudinal mode at low energy emerge with their separation depending strongly on the aspect ratio [59]. In helium nanodroplets, the prevailing multicenter aggregation picture [37] suggests the presence of elongated particles at the employed helium droplet sizes, comprising two (or more) coagulated clusters. Partial melting may occur when two particles are fused together and, in the case of high doping rates, doping material may still be added to coagulated particles [60,61]. Consequently, the exact shape of the particles inside the helium droplet is unknown. However, in order to support the interpretation of the double-peak features, spectra for different particle shapes have been simulated using a boundary element method [62] as implemented in the MATLAB toolbox MNPBEM [63]. Values for the (bulk) dielectric function of potassium have been taken from Refs. [64–66]. Elliptical and rodlike shapes as well as particles that consist of two merged spheres have been considered assuming diameters of 3 nm; the results are included in Appendix E, Fig. 8. The results obtained for the ellipsoidal shape are in best agreement with the experimental spectra. Based on these simulations, it is concluded that the maximum aspect ratio of the formed particles is about 2. In particular, the peak separation observed for potassium clusters in spectra (e) and (g) can be explained by particle shapes with aspect ratios of 1.5 and 1.7, respectively, as can be seen from comparison with the corresponding simulated absorption spectrum (Sim) in Fig. 3. The intensity ratio between the plasmon modes is not captured by the simulation, which is explained by the particle size distribution and the higher sensitivity of the longitudinal mode to the aspect ratio, which results in a spreading of the intensity over a broad spectral range.

The results support an interpretation of the double-peak structure as transversal and longitudinal plasmon modes, indicating that the aspect ratio of the nanoparticle changes gradually from spherical particles to elongated structures. For the employed helium droplet size, this suggests a multicenter aggregation process involving two or three seeds from which a nanoparticle is formed by coagulation. Note that in helium droplets, the formation of elongated structures is facilitated by the attraction of dopants to quantum vortices [67].

IV. CONCLUSIONS

To summarize, potassium clusters isolated in helium nanodroplets are investigated using supercontinuum laser-based beam depletion spectroscopy. The use of this stable turnkey laser system for spectroscopy enables a rapid exploration of large spectral ranges for many different cluster sizes. Taking advantage of this light source, the approach provides insight into the spectra of species ranging from single atoms and molecules to spherical clusters and elongated sub-10-nm nanoparticles. For small clusters indications for an emerging plasmon mode are already found below $n = 20$. With increasing size the plasmon resonance shifts from about 650 toward 600 nm. Size-averaged spectra for larger clusters and nanoparticles reveal a splitting of the plasmon mode beyond $n = 600$. Simulations indicate that the maximum aspect ratio of the formed particles is about 2, suggesting a multicenter aggregation process by which the nanoparticles are formed starting with two to three seeds in the case of helium nanodroplets with mean diameters of about 90 nm.

In the future, the presented approach may be employed to investigate the optical properties of many different materials and material combinations [61] in the core@shell [61] or even the core@shell@shell [68] configuration synthesized in the inert and solvent-free helium droplet environment.

ACKNOWLEDGMENTS

We thank N. Granzow and NKT Photonics for providing the SuperK Extreme supercontinuum laser and the SuperK Varia filter. We are grateful for the MNPBEM MATLAB toolbox developed by Ulrich Hohenester and A. Trügler from Graz University that is available under GNU General Public License, which enabled our simulations. Support by NAWI Graz and the Austrian Science Fund (FWF) under Grant No. P30940-N39 is acknowledged.

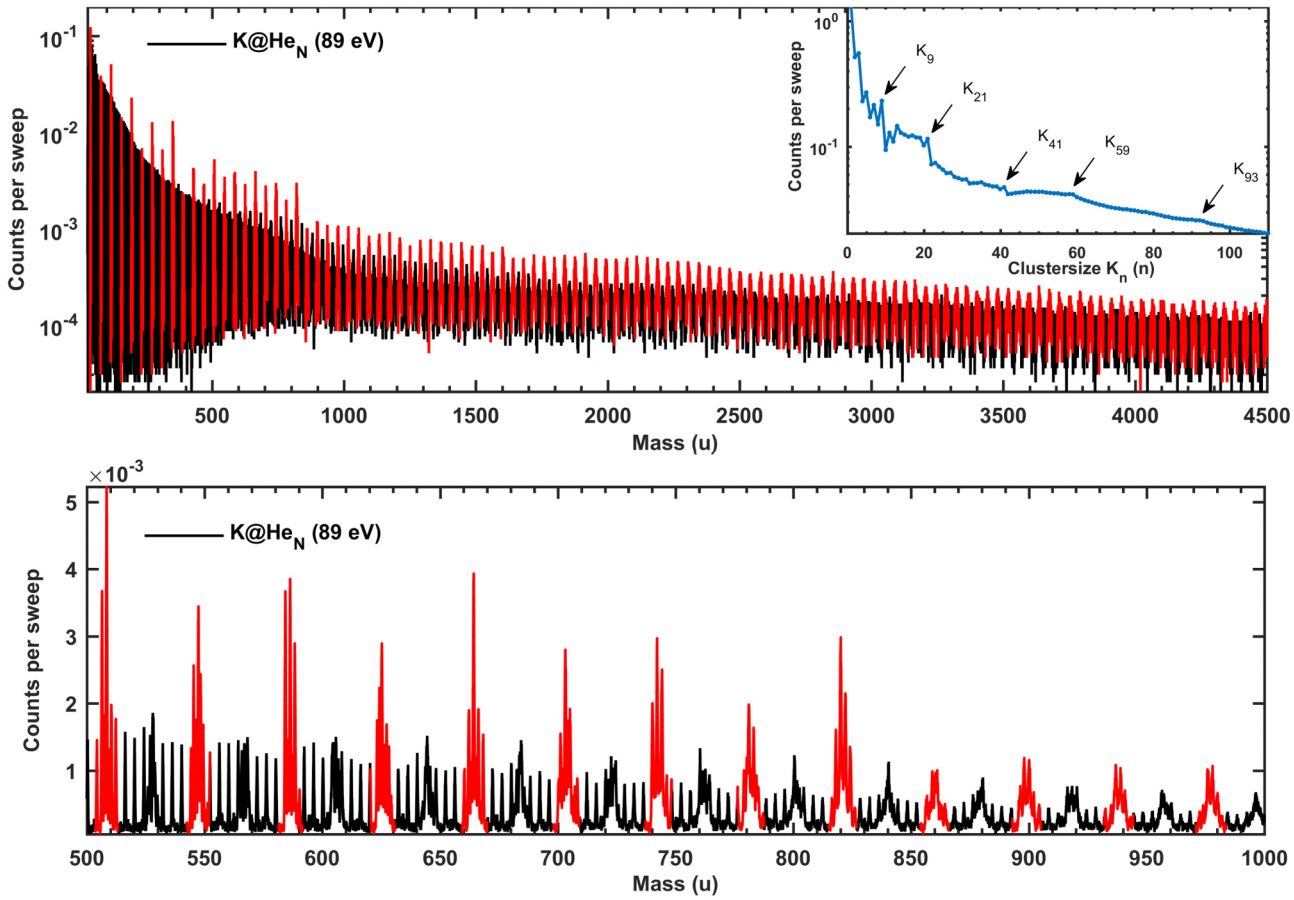

FIG. 4. Top panel: Time-of-flight mass spectrum of potassium doped helium nanodroplets created at 9.5 K and 20 bars stagnation conditions (≈20 nm diameter). Helium nanodroplets are ionized via electron impact ionization. The selected potassium mass windows, separated by $\Delta m = 39$ are represented in red. The inset plot shows the abundance of individual potassium clusters, particularly, stable cluster sizes are marked by arrows. Bottom panel: Time-of-flight mass spectrum for the region from 500 to 1000 amu. Potassium clusters are marked in red, multiple peaks originate from the isotope distribution of ^{39}K (93%) and ^{40}K (7%). The features between the potassium cluster mass peaks are related to helium complexes, potassium clusters with attached water molecules or helium atoms as well as double ionized potassium clusters.

APPENDIX A: TIME-OF-FLIGHT MASS SPECTRUM OF POTASSIUM-DOPED HELIUM NANODROPLETS

Figure 4 shows a typical time-of-flight mass spectrum obtained for potassium-doped helium nanodroplets. An overview spectrum is depicted in the top panel; a zoom into the region from 500 to 1000 amu is presented in the bottom panel. The selected helium droplet source conditions correspond to 9.5 K and 20 bars (≈20 nm mean droplet diameter), an intermediate doping level was adjusted. Ions are created via electron impact ionization at 89 eV electron energy, the electron source has a repetition frequency of 10 kHz. Mass windows corresponding to potassium cluster ions are colored in red. The inset (top panel) shows the integrated ion yield for each marked region. The resulting distribution agrees well with previous results for potassium clusters in helium nanodroplets [32]. For certain K_n cluster sizes, most prominent at $n = 9$, 21, and 41, abrupt drops in the ion yield can be noted. Within the jellium model [11], these magic numbers are explained by electronic shell closures at 9, 21, 41, 59, and 93 potassium atoms for singly ionized clusters, which comprise 8, 20, 40, 58, and 92 valence electrons, respectively. Thus, the recorded spectrum reflects the stability of cluster ions [17].

The presented spectrum was taken using 20 s acquisition time, accumulating 2×10^5 ionization/measurement cycles. This setting was found as best trade-off between signal yield and stability during the wavelength scans because the measurements with the TOF MS are very sensitive to the environmental conditions, such as room temperature or the provided helium gas pressure. Note that during an experimental run a full TOF mass spectrum is recorded for each wavelength step.

APPENDIX B: ELECTRONIC TRANSITIONS OF POTASSIUM ATOMS AND MOLECULES

Electronic transitions of potassium monomers, dimers, and trimers on the surface of helium nanodroplets have been studied in detail previously [25–30,45,46]. This section provides a short summary of investigated transitions and their respec-

TABLE I. List of previously investigated transitions of potassium-doped helium nanodroplets [25–30,45,46].

λ (nm)	Species	Transition
570	K_2	$2\,^3\Pi_g \leftarrow 1\,^3\Sigma_u^+$
617	K_3	$3\,^4E' \leftarrow 1\,^4A_2'$
635	K_2	$1\,^1\Pi_u \leftarrow 1\,^1\Sigma_g^+$
674	K_3	$1\,^4A_1'' \leftarrow 1\,^4A_2'$
715	K_2	$1\,^3\Pi_g \leftarrow 1\,^3\Sigma_u^+$
760	K_1	$4\,^2P_{1/2,3/2} \leftarrow 4\,^2S_{1/2}$
836	K_3	$2\,^4E' \leftarrow 1\,^4A'$

tive positions, which are listed in Table I. A compilation of excitation spectra, adapted from Ref. [46], recorded by laser-induced fluorescence (LIF) spectroscopy, is displayed in Fig. 5. It becomes evident that molecules in their electronic ground state but with different spin configurations are present on helium nanodroplets. An interesting aspect of the spectra presented in the main paper is that a typical wavelength scan from 500 to 840 nm takes about 45 min, much faster than long-range LIF spectroscopy scans with dye lasers.

APPENDIX C: ADDITIONAL INFORMATION ON THE CLUSTER SIZE DEPENDENCE OF THE ABSORPTION PEAK POSITION

Figure 6 shows the position of the absorption band maximum as a function of cluster size for K_n $n = 1$–110 as obtained with the TOF MS (cf. Fig. 2 in the main paper). Individual spectra have been fitted with a Gaussian function, the peak maximum is plotted for each cluster K_n in the figure. A shift towards the blue for increasing cluster size can be identified, in agreement with the prediction of the model described by Kresin [10] (black dashed line). The difference between experiment and model for large clusters is explained by the employed bulk parameters in Ref. [10], which dictate the value towards which the plasmon peak maximum converges.

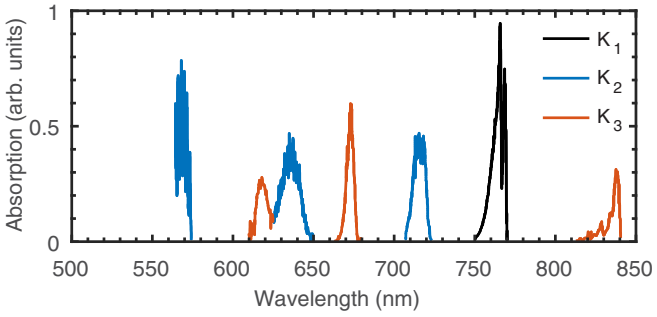

FIG. 5. Compilation of atomic and molecular transitions for potassium-doped helium nanodroplets, recorded by LIF spectroscopy for the monomer (black), dimer (blue), and trimer (red). Adapted from Ref. [46].

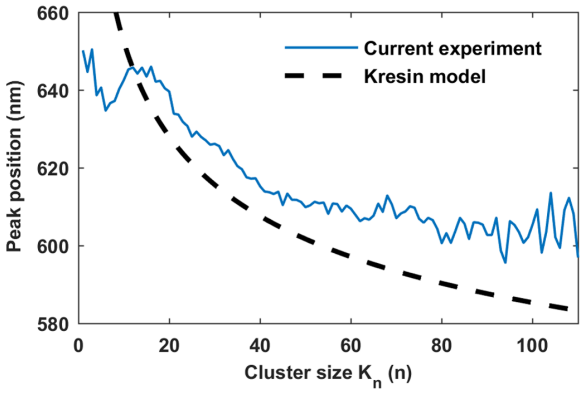

FIG. 6. Position of the absorption maximum as a function of the potassium cluster size. The peak position is obtained from a Gaussian fit to the TOF MS spectra (cf. Fig. 2 in the main paper). The dashed black line represents the results obtained with the Kresin model (Ref. [10]).

APPENDIX D: SIZE ESTIMATION FOR POTASSIUM CLUSTERS

The formation of clusters inside the helium droplet goes along with a release of binding energy $E_K(n)$, which is dissipated by the evaporation of helium atoms. From the number of evaporated helium atoms ΔN, estimated based on the ratio of initial and the attenuated (after doping) helium flux, the approximate number of potassium atoms n constituting a cluster can be calculated by [37]

$$n \approx \Delta N[E_{He}/E_K(n)]. \tag{D1}$$

The energy carried away by a single He atom ($He_N \rightarrow He_{N-1} + He$) is assumed as $E_{He} = 0.6$ meV [61]. The deviation of the binding energy $E_K(n)$ per potassium atom from the bulk value for small n is accounted for by interpolating the calculated binding energy of small clusters [69,70] ($n \leqslant 20$), which converges towards the bulk cohesive energy $E_K(\infty) \approx 0.9$ eV, assuming that $E_K(n)$ is proportional to $n^{-1/3}$. This model is chosen because it reproduces the increasing surface to volume ratio for decreasing cluster sizes. The

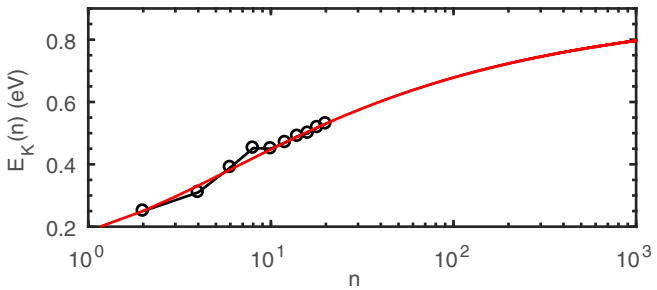

FIG. 7. Employed function (red line) used for the estimation of the binding energy per potassium atom, which accounts for the reduction of binding energy with decreasing cluster size. Calculated values for selected small clusters are represented by black circles, taken from Refs. [69,70]. The function converges toward the bulk cohesive energy $E_K(\infty) \approx 0.9$ eV.

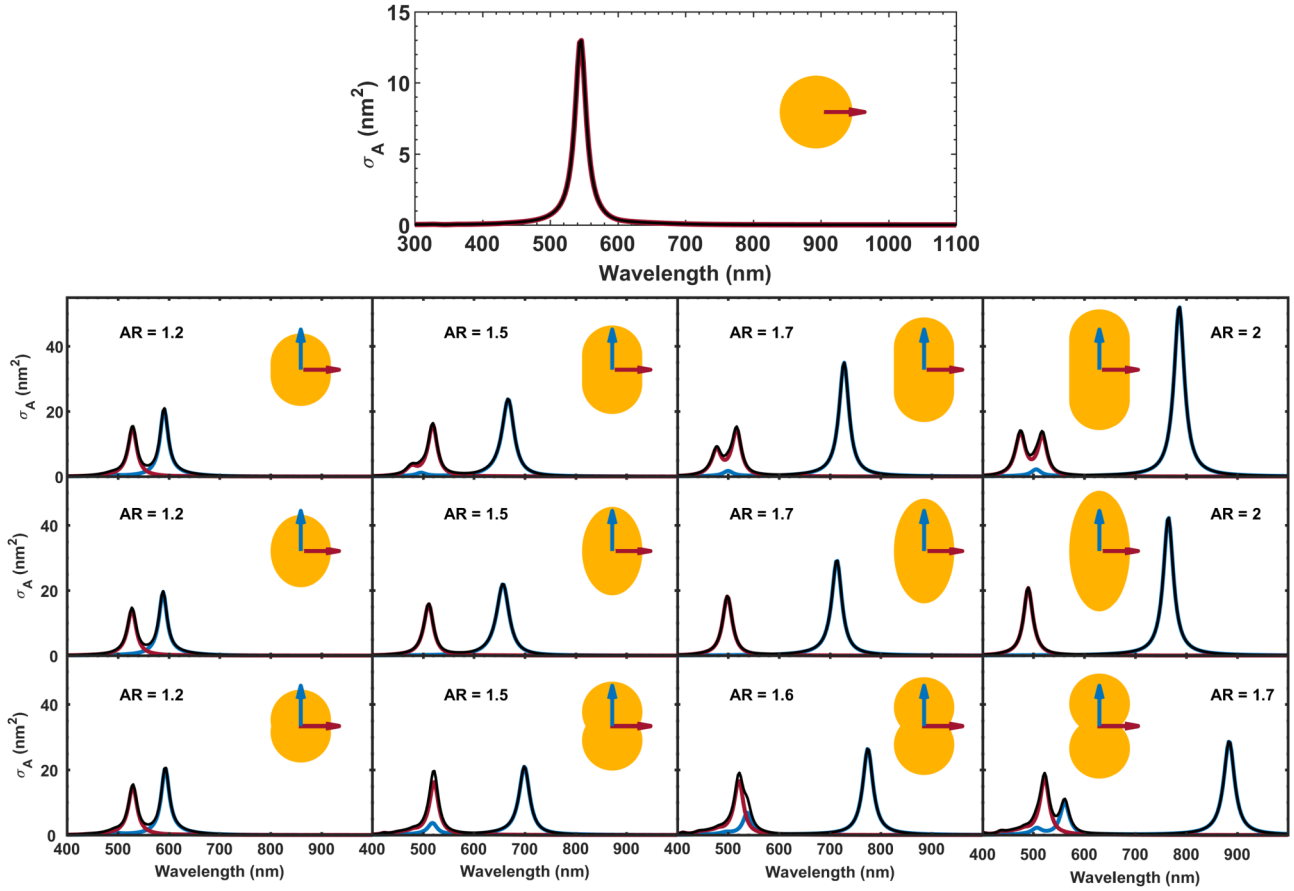

FIG. 8. Calculated absorption spectra of a spherical and several elongated particles with different morphologies and for various aspect ratios (AR)s. The smaller diameter is always 3 nm for all three cases. The red spectrum corresponds to the transversal mode, i.e., when the electric field is aligned perpendicular to the longer particle axis. The blue spectrum corresponds to the longitudinal mode, i.e., the absorption spectrum for the case of the electric field parallel to the longer axis. The black spectrum represents the sum of both contributions. The projected particle shapes are sketched for each calculation, the relative orientation of the electric field is indicated by blue (transversal mode) and red (longitudinal mode) arrows.

employed function used for the estimation of the potassium cluster size is shown in Fig. 7.

APPENDIX E: ADDITIONAL INFORMATION ON THE SIMULATION OF POTASSIUM NANOPARTICLE SPECTRA

To estimate the aspect ratio of potassium nanoparticles created in helium nanodroplets, a series of calculations has been performed using the MNPBEM toolbox [63]. The results are shown in Fig. 8. Three different shapes are considered: A cylindrical nanorod, an ellipsoid and a particle consisting of two merged spheres. For each morphology the calculation has been carried out for different ARs, the result for a sphere (AR = 1) is shown in Fig. 8 (top). The diameter of the particles corresponds to 3 nm. Note that the absolute position of spectral features is not captured accurately by the model, which is based on the macroscopic dielectric function of potassium [64–66]. Size effects, such as the spill out of electrons, are not accounted for. However, the calculation provides qualitative insight into the evolution of the absorption spectrum for different particle shapes at constant diameter, in particular, for varying aspect ratio.

The results show that as soon as the spherical symmetry is lifted, a longitudinal mode at shorter wavelength (higher energy) and a transversal mode at longer wavelengths emerges. With increasing AR, the longitudinal mode shifts to the red whereas the transversal mode shifts towards the blue. The shift is more pronounced for the longitudinal mode, which is, thus, more sensitive to the aspect ratio [59]. A projection of the particle shape assumed in the calculation is shown in each subplot in Fig. 8, together with the relative orientation of the electric field, which is represented by arrows. The results are very similar for all three assumed particle shapes. However, the separation of the two modes in the spectra for nanorods and ellipsoids is virtually indistinguishable. A splitting of the dipolar longitudinal mode as predicted for the rodlike shaped particles (top row) is experimentally not observed. However, this effect may be obscured by the cluster size distribution. The redshift of the longitudinal mode in the merged sphere model is slightly larger, in particular, when approaching an aspect ratio of 2, in the case of which the two spheres barely touch.

Even though the results are very similar for all three cases, the ellipsoidal shape appears to best match the experimental spectra. Consequently, these spectra are presented

in the main paper. However, considering the experimental results as well as the calculations, an aspect ratio beyond 2 is unlikely. Thus, the results suggest the presence of slightly elongated structures at the employed helium droplet sizes and adjusted doping levels, presumably in an ellipsoidal form.

[1] H. Haberland, *Clusters of Atoms and Molecules: Theory, Experiment, and Clusters of Atoms*, 1st ed., Springer Series in Chemical Physics No. 52 (Springer, Berlin, Heidelberg, 1994).

[2] U. Kreibig and M. Vollmer, *Optical Properties of Metal Clusters* (Springer, Berlin/Heidelberg, 2013).

[3] K. Kneipp, M. Moskovits, and H. Kneipp, *Surface-Enhanced Raman Scattering: Physics and Applications* (Springer, Berlin/Heidelberg, 2006).

[4] K. Kneipp, Surface-enhanced raman scattering, Phys. Today **60**(11), 40 (2007).

[5] J. Li, S. K. Cushing, F. Meng, T. R. Senty, A. D. Bristow, and N. Wu, Plasmon-induced resonance energy transfer for solar energy conversion, Nat. Photonics **9**, 601 (2015).

[6] M. Xiao, R. Jiang, F. Wang, C. Fang, J. Wang, and J. C. Yu, Plasmon-enhanced chemical reactions, J. Mater. Chem. A **1**, 5790 (2013).

[7] A. Naldoni, F. Riboni, U. Guler, A. Boltasseva, V. M. Shalaev, and A. V. Kildishev, Solar-powered plasmon-enhanced heterogeneous catalysis, Nanophotonics **5**, 112 (2016).

[8] M. L. Brongersma, N. J. Halas, and P. Nordlander, Plasmon-induced hot carrier science and technology, Nat. Nanotechnol. **10**, 25 (2015).

[9] S. A. Maier, *Plasmonics: Fundamentals and Applications* (Springer, New York, 2007).

[10] V. V. Kresin, Collective resonances and response properties of electrons in metal clusters, Phys. Rep. **220**, 1 (1992).

[11] W. A. de Heer, The physics of simple metal clusters: Experimental aspects and simple models, Rev. Mod. Phys. **65**, 611 (1993).

[12] C. Bréchignac, P. Cahuzac, F. Carlier, and J. Leygnier, Collective excitation in closed-shell potassium cluster ions, Chem. Phys. Lett. **164**, 433 (1989).

[13] N. Dam and W. A. Saunders, Surface-plasmon absorption in singly and doubly charged potassium clusters, Phys. Rev. B **46**, 4205 (1992).

[14] C. Bréchignac, P. Cahuzac, N. Kebaïli, J. Leygnier, and A. Sarfati, Collective Resonance in Large Free Potassium Cluster Ions, Phys. Rev. Lett. **68**, 3916 (1992).

[15] W. A. Saunders, K. Clemenger, W. A. de Heer, and W. D. Knight, Photoionization and shell structure of potassium clusters, Phys. Rev. B **32**, 1366 (1985).

[16] C. Bréchignac, P. Cahuzac, J.-P. Roux, D. Pavolini, and F. Spiegelmann, Adiabatic decomposition of mass-selected alkali clusters, J. Chem. Phys. **87**, 5694 (1987).

[17] C. Bréchignac, P. Cahuzac, and J. P. Roux, Photoionization of potassium clusters: Neutral and ionic cluster stabilities, J. Chem. Phys. **87**, 229 (1987).

[18] S. Saito and M. L. Cohen, Jellium-model calculation for dimer decays of potassium clusters, Phys. Rev. B **38**, 1123 (1988).

[19] H. Abe, K. P. Charlé, B. Tesche, and W. Schulze, Surface plasmon absorption of various colloidal metal particles, Chem. Phys. **68**, 137 (1982).

[20] A. vom Felde, J. Fink, and W. Ekardt, Quantum Size Effects in Excitations of Potassium Clusters, Phys. Rev. Lett. **61**, 2249 (1988).

[21] A. Rosso, G. Öhrwall, I. L. Bradeanu, S. Svensson, O. Björneholm, and M. Tchaplyguine, Photoelectron spectroscopy study of free potassium clusters: Core-level lines and plasmon satellites, Phys. Rev. A **77**, 043202 (2008).

[22] T. Andersson, C. Zhang, A. Rosso, I. Bradeanu, S. Legendre, S. E. Canton, M. Tchaplyguine, G. Öhrwall, S. L. Sorensen, S. Svensson, N. Mårtensson, and O. Björneholm, Plasmon single- and multi-quantum excitation in free metal clusters as seen by photoelectron spectroscopy, J. Chem. Phys. **134**, 094511 (2011).

[23] L. H. Coudert, W. E. Ernst, and O. Golonzka, Hyperfine coupling and pseudorotational motion interaction in Na_3, J. Chem. Phys. **117**, 7102 (2002).

[24] J. Bowlan, A. Liang, and W. A. de Heer, How Metallic are Small Sodium Clusters? Phys. Rev. Lett. **106**, 043401 (2011).

[25] F. Stienkemeier, J. Higgins, C. Callegari, S. I. Kanorsky, W. E. Ernst, and G. Scoles, Spectroscopy of alkali atoms (Li, Na, K) attached to large helium clusters, Z. Phys. D: At., Mol. Clusters **38**, 253 (1996).

[26] J. Higgins, C. Callegari, J. Reho, F. Stienkemeier, W. E. Ernst, K. K. Lehmann, M. Gutowski, and G. Scoles, Photoinduced chemical dynamics of high-spin alkali trimers, Science **273**, 629 (1996).

[27] J. Higgins, C. Callegari, J. Reho, F. Stienkemeier, W. E. Ernst, M. Gutowski, and G. Scoles, Helium cluster isolation spectroscopy of alkali dimers in the triplet manifold, J. Phys. Chem. A **102**, 4952 (1998).

[28] M. Mudrich, O. Bünermann, F. Stienkemeier, O. Dulieu, and M. Weidemüller, Formation of cold bialkali dimers on helium nanodroplets, Eur. Phys. J. D **31**, 291 (2004).

[29] J. Nagl, G. Auböck, A. W. Hauser, O. Allard, C. Callegari, and W. E. Ernst, Heteronuclear and Homonuclear High-Spin Alkali Trimers on Helium Nanodroplets, Phys. Rev. Lett. **100**, 063001 (2008).

[30] J. Nagl, G. Auböck, A. W. Hauser, O. Allard, C. Callegari, and W. E. Ernst, High-spin alkali trimers on helium nanodroplets: Spectral separation and analysis, J. Chem. Phys. **128**, 154320 (2008).

[31] C. P. Schulz, P. Claas, D. Schumacher, and F. Stienkemeier, Formation and Stability of High-Spin Alkali Clusters, Phys. Rev. Lett. **92**, 013401 (2004).

[32] L. An der Lan, P. Bartl, C. Leidlmair, H. Schöbel, S. Denifl, T. D. Märk, A. M. Ellis, and P. Scheier, Submersion of potassium clusters in helium nanodroplets, Phys. Rev. B **85**, 115414 (2012).

[33] M. Renzler, M. Harnisch, M. Daxner, L. Kranabetter, M. Kuhn, P. Scheier, and O. Echt, Fission of multiply charged alkali clusters in helium droplets – Approaching the rayleigh limit, Phys. Chem. Chem. Phys. **18**, 10623 (2016).

[34] C. Stark and V. V. Kresin, Critical sizes for the submersion of alkali clusters into liquid helium, Phys. Rev. B **81**, 085401 (2010).

[35] F. Federmann, K. Hoffmann, N. Quaas, and J. P. Toennies, Spectroscopy of extremely cold silver clusters in helium droplets, Eur. Phys. J. D **9**, 11 (1999).

[36] P. Radcliffe, A. Przystawik, T. Diederich, T. Döppner, J. Tiggesbäumker, and K.-H. Meiwes-Broer, Excited-State Relaxation of Ag_8 Clusters Embedded in Helium Droplets, Phys. Rev. Lett. **92**, 173403 (2004).

[37] E. Loginov, L. F. Gomez, N. Chiang, A. Halder, N. Guggemos, V. V. Kresin, and A. F. Vilesov, Photoabsorption of $Ag_N(N \sim 6-6000)$ Nanoclusters Formed in Helium Droplets: Transition from Compact to Multicenter Aggregation, Phys. Rev. Lett. **106**, 233401 (2011).

[38] L. F. Gomez, E. Loginov, A. Halder, V. V. Kresin, and A. F. Vilesov, Formation of unusual copper clusters in helium nanodroplets, Int. J. Nanosci. **12**, 1350014 (2013).

[39] P. Thaler, A. Volk, D. Knez, F. Lackner, G. Haberfehlner, J. Steurer, M. Schnedlitz, and W. E. Ernst, Synthesis of nanoparticles in helium droplets—a characterization comparing mass-spectra and electron microscopy data, J. Chem. Phys. **143**, 134201 (2015).

[40] J. P. Toennies and A. F. Vilesov, Superfluid helium droplets: A uniquely cold nanomatrix for molecules and molecular complexes, Angew. Chem. Int. Ed. **43**, 2622 (2004).

[41] C. Callegari and W. E. Ernst, Helium droplets as nanocryostats for molecular spectroscopy—from the vacuum ultraviolet to the microwave regime, in *Handbook of High-resolution Spectroscopy*, edited by M. Quack and F. Merkt (John Wiley & Sons, Chichester, 2011).

[42] M. Lewerenz, B. Schilling, and J. P. Toennies, Successive capture and coagulation of atoms and molecules to small clusters in large liquid helium clusters, J. Chem. Phys. **102**, 8191 (1995).

[43] M. Theisen, F. Lackner, and W. E. Ernst, Rb and Cs oligomers in different spin configurations on helium nanodroplets, J. Phys. Chem. A **115**, 7005 (2011).

[44] L. F. Gomez, S. M. O. O'Connell, C. F. Jones, J. Kwok, and A. F. Vilesov, Laser-induced reconstruction of Ag clusters in helium droplets, J. Chem. Phys. **145**, 114304 (2016).

[45] J. Higgins, W. E. Ernst, C. Callegari, J. Reho, K. K. Lehmann, G. Scoles, and M. Gutowski, Spin Polarized Alkali Clusters: Observation of Quartet States of the Sodium Trimer, Phys. Rev. Lett. **77**, 4532 (1996).

[46] J. Nagl, Spectroscopic investigations of homo- and heteronuclear molecules of K and Rb on the surface of argon and helium clusters, Ph.D. thesis, Graz University of Technology, Graz, 2008.

[47] F. Ancilotto, P. B. Lerner, and M. W. Cole, Physics of solvation, J. Low Temp. Phys. **101**, 1123 (1995).

[48] F. Ancilotto, M. Barranco, F. Coppens, J. Eloranta, N. Halberstadt, A. Hernando, D. Mateo, and M. Pi, Density functional theory of doped superfluid liquid helium and nanodroplets, Int. Rev. Phys. Chem. **36**, 621 (2017).

[49] S. Denifl, Formation of cations and anions upon electron interaction with (doped) helium droplets, Eur. Phys. J.: Spec. Top. **222**, 2017 (2013).

[50] S. Yang, S. M. Brereton, M. D. Wheeler, and A. M. Ellis, Soft or hard ionization of molecules in helium nanodroplets? An electron impact investigation of alcohols and ethers, Phys. Chem. Chem. Phys. **7**, 4082 (2005).

[51] M. Lasserus, M. Schnedlitz, R. Messner, F. Lackner, W. E. Ernst, and A. W. Hauser, Vanadium(V) oxide clusters synthesized by sublimation from bulk under fully inert conditions, Chem. Sci. **10**, 3473 (2019).

[52] L. F. Gomez, E. Loginov, R. Sliter, and A. F. Vilesov, Sizes of large He droplets, J. Chem. Phys. **135**, 154201 (2011).

[53] F. Lackner and W. E. Ernst, Photoinduced molecule formation of spatially separated atoms on helium nanodroplets, J. Phys. Chem. Lett. **9**, 3561 (2018).

[54] D. Melnikau, D. Savateeva, A. Sánchez-Iglesias, M. Grzelczak, L. M. Liz-Marzán, M. K. Schmidt, R. Estiban, J. Aizpurua, and Y. P. Rakovich, Strong excitonic-plasmonic coupling in hybrid system of metal nanoparticles and J-aggregates of organic dye, in *2015 17th International Conference on Transparent Optical Networks (ICTON)* (IEEE, Piscataway, NJ, 2015), pp. 1–4.

[55] D. Shajari, A. Bahari, P. Gill, and M. Mohseni, Synthesis and tuning of gold nanorods with surface plasmon resonance, Opt. Mater. (Amsterdam) **64**, 376 (2017).

[56] X. Huang, I. H. El-Sayed, W. Qian, and M. A. El-Sayed, Cancer cell imaging and photothermal therapy in the near-infrared region by using gold nanorods, J. Am. Chem. Soc. **128**, 2115 (2006).

[57] D.-S. Wang, F.-Y. Hsu, and C.-W. Lin, Surface plasmon effects on two photon luminescence of gold nanorods, Opt. Express **17**, 11350 (2009).

[58] A. Schiffmann, D. Knez, F. Lackner, M. Lasserus, R. Messner, M. Schnedlitz, G. Kothleitner, F. Hofer, and W. E. Ernst, Ultra-thin h-BN substrates for nanoscale plasmon spectroscopy, J. Appl. Phys. **125**, 023104 (2019).

[59] S. Link, M. B. Mohamed, and M. A. El-Sayed, Simulation of the optical absorption spectra of gold nanorods as a function of their aspect ratio and the effect of the medium dielectric constant, J. Phys. Chem. B **103**, 3073 (1999).

[60] A. Volk, P. Thaler, D. Knez, A. W. Hauser, J. Steurer, W. Grogger, F. Hofer, and W. E. Ernst, The impact of doping rates on the morphologies of silver and gold nanowires grown in helium nanodroplets, Phys. Chem. Chem. Phys. **18**, 1451 (2016).

[61] W. E. Ernst and A. W. Hauser, Metal clusters synthesized in helium droplets: Structure and dynamics from experiment and theory, Phys. Chem. Chem. Phys. **23**, 7553 (2021).

[62] F. J. García de Abajo and A. Howie, Retarded field calculation of electron energy loss in inhomogeneous dielectrics, Phys. Rev. B **65**, 115418 (2002).

[63] U. Hohenester and A. Trügler, MNPBEM – A matlab toolbox for the simulation of plasmonic nanoparticles, Comput. Phys. Commun. **183**, 370 (2012).

[64] N. V. Smith, Optical constants of sodium and potassium from 0.5 to 4.0 eV by split-beam ellipsometry, Phys. Rev. **183**, 634 (1969).

[65] U. S. Whang, E. T. Arakawa, and T. A. Callcott, Optical properties of K between 4 and 10.7 eV and comparison with Na, Rb, and Cs, Phys. Rev. B **6**, 2109 (1972).

[66] J. Monin and G. A. Boutry, Optical and photoelectric properties of alkali metals, Phys. Rev. B **9**, 1309 (1974).

[67] O. Gessner and A. F. Vilesov, Imaging quantum vortices in superfluid helium droplets, Annu. Rev. Phys. Chem. **70**, 173 (2019).

[68] R. Messner, W. E. Ernst, and F. Lackner, Shell-isolated Au nanoparticles functionalized with rhodamine B fluorophores in helium nanodroplets, J. Phys. Chem. Lett. **12**, 145 (2021).

[69] S. Ishii, K. Ohno, Y. Kawazoe, and S. G. Louie, *Ab initio GW* quasiparticle calculation of small alkali-metal clusters, Phys. Rev. B **65**, 245109 (2002).

[70] A. Banerjee, T. K. Ghanty, and A. Chakrabarti, Ab initio studies of properties of small potassium clusters, J. Phys. Chem. A **112**, 12303 (2008).